Dynamic spin fluctuations in stage-2 $NiCl_2$ graphite intercalation compound

1998 J. Phys.: Condens. Matter 10 5399

(http://iopscience.iop.org/0953-8984/10/24/017)

J. Phys.: Condens. Matter **10** (1998) 5399–5419. Printed in the UK PII: S0953-8984(98)92182-8

Dynamic spin fluctuations in stage-2 $NiCl_2$ graphite intercalation compound

Itsuko S Suzuki and Masatsugu Suzuki

Department of Physics, State University of New York at Binghamton, Binghamton, NY 13902-6016, USA

Received 3 March 1998

Abstract. Stage-2 $NiCl_2$ GIC is a quasi-two-dimensional XY-like ferromagnet with very weak antiferromagnetic interplanar exchange interaction. This compound undergoes two magnetic phase transitions at T_{cu} (=20.5 ± 0.2 K) and T_{cl} (=17.2 K). Between T_{cu} and T_{cl} a two-dimensional long range spin order is established within each island in the intercalate layers. Below T_{cl} there appears a three-dimensional antiferromagnetic ordered phase. The dynamic aspect of spin ordering in this compound has been studied employing the temperature, frequency and field dependence of dispersion χ' and absorption χ'' acquired using an AC SQUID magnetometer. The absorption χ'' shows a complicated frequency dependence near T_{cu} and T_{cl}, suggesting two kinds of relaxation time associated with intraisland fluctuation (τ_{in}) and interisland fluctuation (τ_{out}): τ_{out} is much longer than τ_{in}.

1. Introduction

Stage-2 $NiCl_2$ graphite intercalation compound approximates a quasi-two-dimensional (2D) XY-like ferromagnet with an extremely weak antiferromagnetic interplanar exchange interaction. Structurally there are two graphite layers separating neighbour $NiCl_2$ layers in a periodic arrangement along the c axis. Magnetic phase transitions of this compound have been examined in detail by various kinds of measurement [1–17] such as AC magnetic susceptibility, magnetization, nonlinear magnetic susceptibility, neutron scattering and so on. This compound undergoes two magnetic phase transitions at T_{cu} and T_{cl}. The values of T_{cu} and T_{cl} are different depending on its definition and method of measurement: $T_{cu} = 20.2$ K and $T_{cl} = 18.1$ K (Karimov *et al* [1]), $T_{cu} = 19.40$ K and $T_{cl} = 17.3$ K (Suzuki and Ikeda [7]), $T_{cu} = 21.3$ K and $T_{cl} = 18.0$ K (Suzuki *et al* [9]), $T_{cu} = 22.0$ K and $T_{cl} = 17.5$ K (Suematsu *et al* [11]) $T_{cu} = 21 \pm 1$ K and $T_{cl} = 19 \pm 1$ K (Wiesler *et al* [14]) and $T_{cu} = 21$ K and $T_{cl} = 17$ K (Matsuura and Hagiwara [15]).

The intercalate layers of this compound are formed of small islands. The island periphery provides acceptor sites for charges which are transferred from graphite layers during the intercalation process. This finite size of small islands is a crucial element in the magnetic phase transition of this compound. The effective interplanar exchange interaction J'_{eff} between spins over the in-plane spin correlation length ξ_a in adjacent magnetic intercalate layers is described by $J'_{eff} = J'(\xi_a/a)^2$, where J' is the interplanar exchange interaction and a is the in-plane lattice constant. The growth of ξ_a is limited by the island size as the temperature is decreased. Suppression of the increase in J'_{eff} leads to the realization of 2D spin ordering between T_{cu} and T_{cl}. Below T_{cl} there occurs a 3D spin ordering where the 2D ferromagnetic layers are antiferromagnetically stacked along the c axis. Experimentally

0953-8984/98/245399+21$19.50

this has been revealed through magnetic neutron scattering along the $\boldsymbol{c}^*$ axis, where $\boldsymbol{c}^*$ ($|\boldsymbol{c}^*| = 2\pi/d$) is the reciprocal lattice vector parallel to the c axis and d is the c-axis repeat distance. Below T_{cl} the antiferromagnetic Bragg peaks appear at the scattering wave vector $\boldsymbol{Q} = \ell\boldsymbol{c}^*$ with $\ell = 1/2,\ 3/2,\ 5/2$ and $7/2$, showing the antiferromagnetic spin ordering along the c axis. Between T_{cu} and T_{cl} a smooth magnetic ridge appears along the $\boldsymbol{c}^*$ direction, showing the 2D ferromagnetic spin ordering in the c plane [14].

In this paper we have undertaken an extensive study on the magnetic properties of this compound using SQUID DC magnetization and SQUID AC magnetic susceptibility. The dispersion χ' and absorption χ'' are measured as a function of temperature and frequency with and without an external magnetic field, using an AC SQUID magnetometer. Between T_{cu} (=17.2 K) and T_{cl} (=20.5 ± 0.2 K) the interisland correlation is still random within each intercalate layer. The magnetization of each island will fluctuate and change direction relative to other islands in a certain characteristic time scale depending on the island size and interisland interaction. There are two kinds of relaxation time associated with intraisland fluctuation (τ_{in}) and interisland fluctuation (τ_{out}). The relaxation time τ_{out} is assumed to be much longer than the relaxation time τ_{in}. The contribution of the intraisland and interisland fluctuations to χ'' may be observed separately if χ'' is measured at different frequencies. In fact we show that the complicated frequency dependence of χ'' observed near T_{cu} and T_{cl} can be explained in terms of a simple model that both intraisland and interisland fluctuations have relaxation of Debye type with relaxation times τ_{in} and τ_{out}, respectively. The magnetic properties of this compound such as a spin Hamiltonian and the effect of magnetic field on magnetic phase transitions are also examined from magnetization and magnetic susceptibility.

2. Spin Hamiltonian and its related properties

The spin Hamiltonian of stage-2 $NiCl_2$ GIC with spin S (=1) can be described by [13]

$$\mathcal{H} = -2J\sum_{\langle i,j\rangle}\boldsymbol{S}_i\cdot\boldsymbol{S}_j + D\sum_i (S_i^z)^2 - 2J'\sum_{\langle i,m\rangle}\boldsymbol{S}_i\cdot\boldsymbol{S}_m \tag{1}$$

where the z axis coincides with the c axis, J (>0) is the ferromagnetic intraplanar exchange interaction, D (>0) is the single ion anisotropy term, and J' (<0) is the antiferromagnetic interplanar exchange interaction. For convenience the equivalent interaction fields at 0 K are defined as $H_A^{out} = DS/g_c\mu_B$, $H_E' = 2z'|J'|S/g_a\mu_B$, $H_E = 2zJS/g_a\mu_B$ and $H_{SF} = [2H_A^{in}H_E']^{1/2}$ where g_a and g_c are the g values along the c plane and c axis ($g_a = 2.156\pm0.002$ and $g_c = 2.096\pm0.002$ at 300 K [13]). H_E is the intraplanar exchange field, H_E' the interplanar exchange field, H_{SF} the spin flop field, H_A^{in} the anisotropy field in the c plane, H_A^{out} the anisotropy field along the c axis and z and z' the numbers of interacting neighbours in and between the c plane, respectively ($z = z' = 6$).

In terms of the spin Hamiltonian (1) the magnetic susceptibility at 0 K can be derived as $\chi_a = N_A(g_a\mu_B)^2/4z'|J'|$ and $\chi_c = N_A(g_c\mu_B)^2/(2D+4z'|J'|)$. Then characteristic magnetic field H_0^c is defined as $H_0^c = 2[H_A^{out} + (g_a/g_c)H_E']$ where the magnetization $M_c = \chi_c H$ is equal to the saturation magnetization M_c^s ($=N_A g_c\mu_B S$). Similarly the characteristic magnetic field H_0^a is defined as $H_0^a = 2H_E'$ where the magnetization $M_a = \chi_a H$ is equal to the saturation magnetization M_a^s ($=N_A g_a\mu_B S$). Since H_E' is assumed to be much smaller than H_A^{out}, H_0^c is approximately equal to $H_0^c \approx 2H_A^{out}$.

For comparison the magnetic properties of the pristine $NiCl_2$ are presented here. It undergoes an antiferromagnetic phase transition at the Néel temperature $T_N = 52.3$ K [18]. The spin Hamiltonian is also given by (1). The ferromagnetic intraplanar interaction J and

the effective magnetic moment P_{eff} are estimated as $J = 8.53$ K and $P_{eff} = 3.30\ \mu_B$ from Curie–Weiss temperature $\Theta = 68.2$ K and Curie–Weiss constant $C = 1.36$ emu K mol^{-1} [19]. The values of D and J' are determined as $D = 0.40$ K and $J' = -0.78$ K from the antiferromagnetic resonance [20] and magnetic susceptibility [21]. From the in-plane spin wave dispersion relation, Lindgård *et al* [22] deduce the ferromagnetic nearest neighbour (n.n.) and antiferromagnetic next nearest neighbour (n.n.n.) intraplanar exchange interactions $J_{n.n.} = 10.85$ K and $J_{n.n.n.} = -2.425$ K in our definition of spin Hamiltonian, which correspond to one-half of those originally reported by Lindgård *et al* [22]. Note that the sum ($J_{n.n.} + J_{n.n.n.} = 8.425$ K) is close to the value of J derived from Θ. Thus we can estimate $D/J = 4.78 \times 10^{-2}$, $H_A^{out} = 2.84$ kOe and $H'_E = 63.8$ kOe.

3. Experimental procedure

A sample of stage-2 $NiCl_2$ GIC was prepared from single crystal of kish graphite (SCKG) by vapour reaction of anhydrated $NiCl_2$ in a chlorine atmosphere with a gas pressure of $\approx$740 Torr. The reaction was continued at 560 °C for one month. The stage structure of this compound was confirmed from (00l) x-ray diffraction to be well defined stage 2: the c-axis repeat distance is 12.78 ± 0.02 Å. The $NiCl_2$ layer forms a triangular lattice with the in-plane lattice constant 3.46 ± 0.01 Å close to that for the pristine $NiCl_2$ (3.465 Å) [14]. The $NiCl_2$ layer is incommensurate with the graphite layer and is rotated by 30° with respect to the graphite layer. The stoichiometry was determined from a weight uptake measurement as $C_{8.33\pm0.02}NiCl_2$. The ideal stoichiometry is estimated as $C_{7.91}NiCl_2$. Therefore the filling factor is estimated as 97% if the sample has no stage mixture. The sample used in the present work has a rectangular form of $3 \times 3 \times 0.2$ mm^3.

The AC magnetic susceptibility and DC magnetization were measured using a SQUID magnetometer (Quantum Design, MPMS XL-5) with an ultra-low field capability option.

(i) *AC magnetic susceptibility.* The sample was cooled from 298 K to 8 K in a zero magnetic field (less than 3 mOe). Then the temperature (T) dependence of dispersion χ' and absorption χ'' was measured between 8 K and 25 K in the absence and presence of external magnetic field (H). The amplitude of AC magnetic field h is 50 mOe and the frequency (f) range is between 0.02 Hz and 1 kHz.

(ii) *DC magnetization.* The sample was cooled from 298 K to 1.9 K in a zero magnetic field. Then an external magnetic field H (=1 Oe) is applied at 1.9 K. The zero field cooled (ZFC) magnetization was measured with increasing temperature from 1.9 K to 30 K and the field cooled (FC) magnetization was measured with decreasing temperature from 30 K to 1.9 K.

(iii) The DC magnetic susceptibility was also measured while the sample was cooled from 300 K to 2 K in the presence of H (=1 kOe).

4. Results

Figure 1(a) shows the T-dependence of DC magnetic susceptibility χ_a ($=M_a/H$) and χ_c ($=M_c/H$) at $H = 1$ kOe for stage-2 $NiCl_2$ GIC, where M_a and M_c are the magnetizations along the c plane and the c axis. The deviation of χ_a from χ_c occurs at least below 60 K, suggesting that short range spin order appears below this temperature. The susceptibility χ_c shows a peak around 18 K, while χ_a increases with decreasing temperature.

The DC magnetic susceptibility χ_a and χ_c obey a Curie–Weiss law in the T range between 150 and 300 K. The least squares fit of the data to the Curie–Weiss law yields the

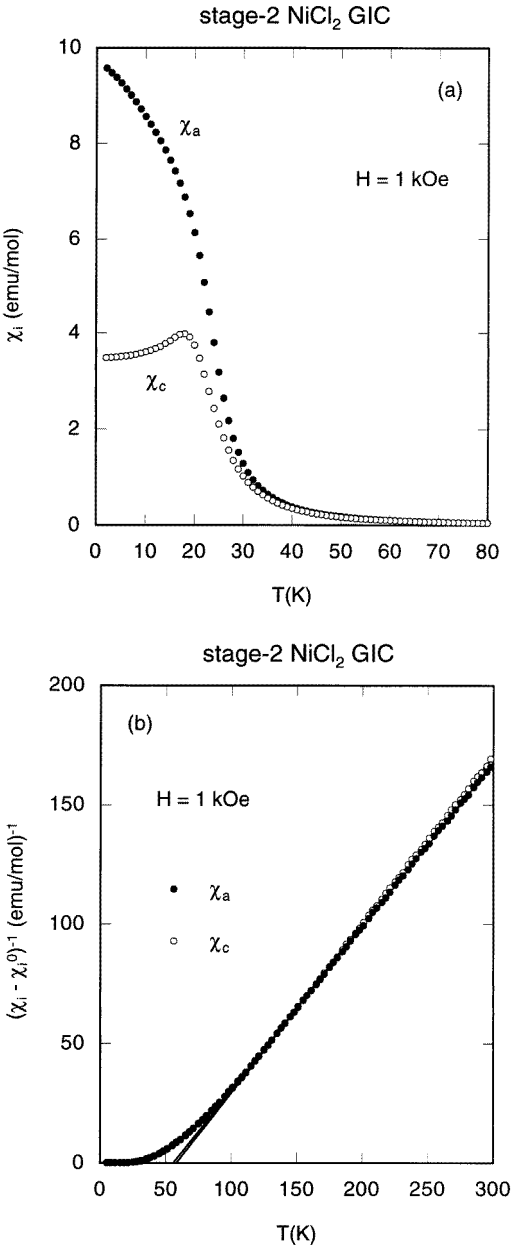

Figure 1. (a) T dependence of χ_a ($H \perp c$) and χ_c ($H \parallel c$) for stage-2 $NiCl_2$ GIC. $H = 1$ kOe. (b) T dependence of reciprocal susceptibility $(\chi_i - \chi_i^0)^{-1}$ for $i = a$ (●) and c (○). $H = 1$ kOe. The straight line denotes a least squares fit of the data to the Curie–Weiss law. (c) H dependence of M_a ($H \perp c$) and M_c ($H \parallel c$) at $T = 1.9$ K. The inset shows the H dependence of M_a/H.

Curie–Weiss temperature $\Theta_a = 58.07 \pm 0.38$ K and Curie–Weiss constant $C_a = 1.419 \pm 0.008$ emu K mol^{-1} for the c plane and $\Theta_c = 55.66 \pm 0.36$ K and $C_c = 1.456 \pm 0.008$ emu K mol^{-1} for the c axis. Figure 1(b) shows the T dependence of reciprocal susceptibility $(\chi_i - \chi_i^0)^{-1}$ for $i = a$ and c, where χ_i^0 is a temperature-independent susceptibility determined

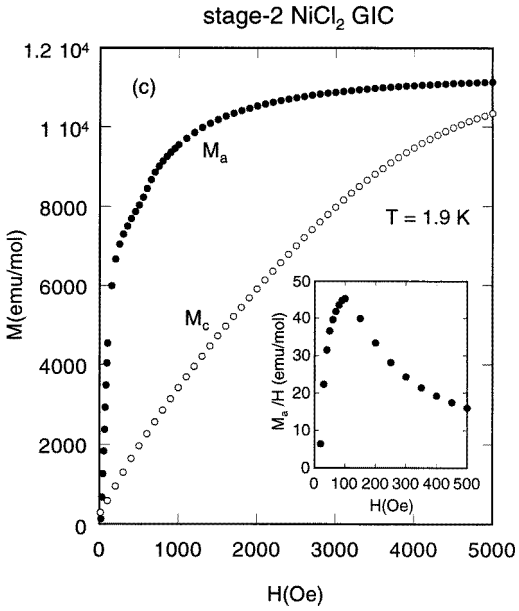

Figure 1. (Continued)

from the least squares fit. Our value of Θ_a is a little smaller than that previously reported: $\Theta_a = 70 \pm 1$ K (Suematsu *et al* [11]) and $\Theta_a = 65$ K (Flandrois *et al* [6]) for stage-2 $NiCl_2$ GIC and $\Theta_a = 60$ K (Flandrois *et al* [23]) for stage-1 $NiCl_2$ GIC. The intraplanar exchange interaction J is estimated as $J = 3\Theta_a/[2zS(S+1)] = 7.26 \pm 0.05$ K. The effective magnetic moment is calculated as $P^a_{eff} = 3.369\ \mu_B$, which is almost the same as those previously reported: $P_{eff} = 3.3\ \mu_B$ (Flandrois *et al* [6]) and $P_{eff} = 3.29\ \mu_B$ (Suematsu *et al* [11]). The value of P_{eff} is a little larger than the theoretical value for complete orbital quenching ($=2.83\ \mu_B$). Ni ions exist as divalent ions in the $NiCl_2$ intercalate layer.

Figure 1(c) shows the H dependence of magnetization M_a and M_c at 1.9 K. The magnetization M_a drastically increases with increasing field and reaches a saturated value M^s_a ($=1.204 \times 10^4$ emu mol^{-1}) at relatively low fields. Here we note that the measurement of M_c against H was made at 1.9 K with H varied from 0 to 5 kOe after the measurement of χ_c against H was made at $H = 1$ kOe with T varied from 298 to 1.9 K. Therefore the value of M_c at $H = 0$ in figure 1(c) corresponds to a remanent magnetization. We also notice a slight kink in M_a around $H = 500$ Oe, which is of the same order as the critical field H'_E for stage-1 $NiCl_2$ GIC [23, 24]. This may suggest that slight stage-1 fractions exist in our sample, in spite of the fact that our sample was confirmed to be well defined stage 2 from the (00l) x-ray diffraction measurement. The value of M_c is smaller than that of M_a for $0 < H \leqslant 5$ kOe, indicating that spins lie in the c plane. The values of H^{out}_A and H'_E can be derived from these data. As described in section 2, the fields H^a_0 (H^c_0) are defined as the fields where the tangential line of the magnetization–H curve at $H = 0$ intersects the line $M = M^s_a$ (M^s_c). In figure 1(c) we can estimate $H^a_0 \approx 100$ Oe and $H^c_0 = 4$ kOe, leading to $H'_E = 50$ Oe and $H^{out}_A = 2$ kOe. These values are in good agreement with those previously reported by Suzuki and Ikeda [7]. In the inset of figure 1(c) we show the plot of M_a/H at 1.9 K as a function of H. It has a peak around $H = 100$ Oe, suggesting that H'_E is of the order of 50 Oe. Then the parameters D and J' are determined as $D = 0.28$ K and

$J' = -6 \times 10^{-4}$ K for $z' = 6$ and $H'_E = 50$ Oe. The ratio D/J is estimated as 3.86×10^{-2} close to that (4.78×10^{-2}) for pristine $NiCl_2$.

Figure 2 shows the T dependence of FC magnetization M_a^{FC} and ZFC magnetization M_a^{ZFC} in the presence of $H = 1$ Oe along the c plane. The magnetization M_a^{ZFC} has a broad peak at 18.5 K, while M_a^{FC} drastically increases with decreasing temperature. The deviation of M_a^{ZFC} from M_a^{FC} occurs below $T_f = 21.8$ K, indicating that an irreversible effect of magnetization occurs below T_f.

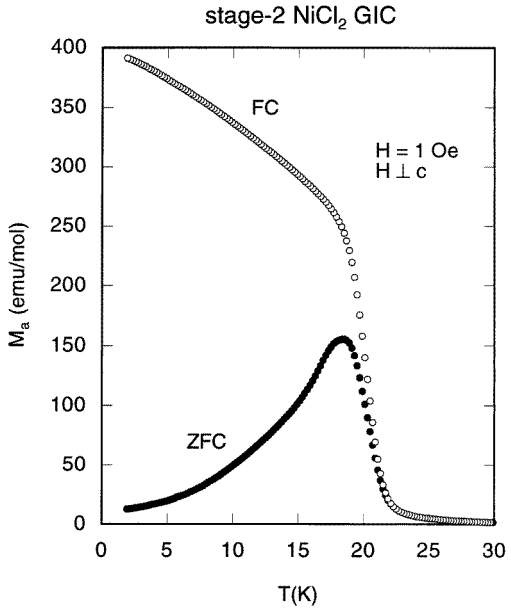

Figure 2. T dependence of M_a^{FC} (○) and M_a^{ZFC} (●). $H \perp c$. $H = 1$ Oe.

Figures 3(a) and (b) show the T dependence of dispersion χ'_{aa} and absorption χ''_{aa} for various frequencies at $H = 0$, respectively. The dispersion χ'_{aa} has a single broad peak at 18.8 K. This peak temperature does not change with frequency, while the magnitude of χ'_{aa} is dependent on frequency. The absorption χ''_{aa} has a broad peak at 17.2 K and a shoulder around 20.5 K for $f = 0.02$ Hz. The broad peak shifts to the high temperature side with increasing frequency (17.8 K for $f = 1$ kHz). The magnitude of χ''_{aa} between 17.2 K and 20.5 K is strongly dependent on frequency. These results are similar to those of stage-2 $CoCl_2$ GIC [25]. (i) The absorption χ''_{aa} of stage-2 $CoCl_2$ GIC has two peaks at 6.9 and 8.9 K at $f = 0.1$ Hz, which are defined as critical temperatures T_{cl} and T_{cu}, respectively. (ii) The critical temperature T_{cl} slightly increases with increasing frequency, while T_{cu} remains unchanged. (iii) The dispersion χ'_{aa} has a peak at 8.4 K between T_{cl} and T_{cu}. Since the magnetic phase transitions of stage-2 $NiCl_2$ GIC are similar to those of stage-2 $CoCl_2$ GIC, it is reasonable to define T_{cl} and T_{cu} as $T_{cl} = 17.2$ K and $T_{cu} = 20.5 \pm 0.2$ K for stage-2 $NiCl_2$ GIC. Note that the uncertainty of T_{cu} arises partly from that in the temperature for the shoulder in χ''_{aa}.

Figures 4(a) and (b) show the T dependence of χ'_{cc} and χ''_{cc} for various frequencies at $H = 0$, respectively. Here we show only the data for $0.1 \leqslant f \leqslant 3$ Hz. A sample holder used for the measurement of χ'_{cc} and χ''_{cc} has an appreciable frequency-dependent baseline to the AC susceptibility for $f > 10$ Hz. The dispersion χ'_{cc} has a single broad peak at

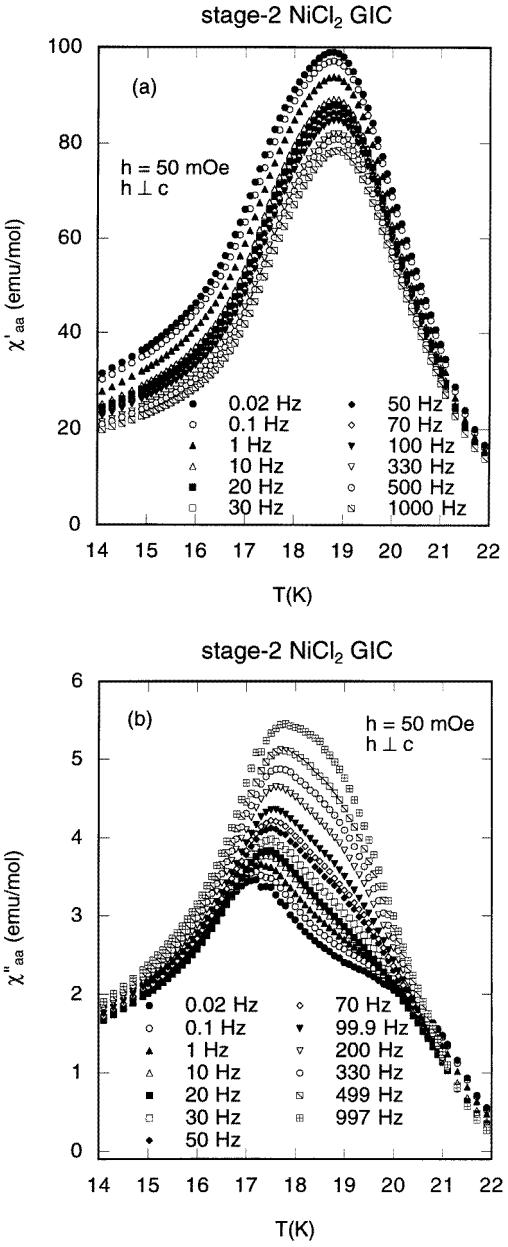

Figure 3. T dependence of (a) χ'_{aa} and (b) χ''_{aa} at various frequencies. $h = 50$ mOe. $h \perp c$.

18.9 K, independent of frequency for $0.1 \leqslant f \leqslant 1000$ Hz. The absorption χ''_{cc} has two peaks at 17.1 K and 19.3 K for $f = 0.1$ Hz, which approximately coincide with T_{cl} and the peak temperature of χ'_{aa}, respectively.

Figure 5 shows the f dependence of peak temperatures T_p for χ'_{aa}, χ''_{aa}, χ'_{cc} and χ''_{cc}, where the temperature for the shoulder of χ''_{aa} is not included. The peak temperature of χ''_{aa} and χ''_{cc} corresponding to T_{cl} slightly increases with increasing frequency. This feature is

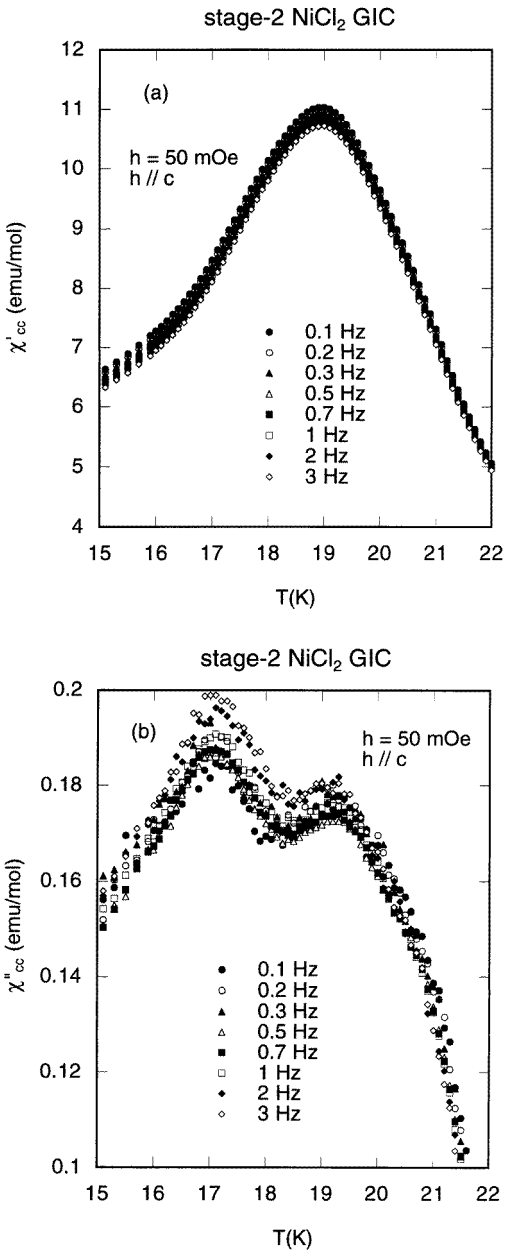

Figure 4. T dependence of (a) χ'_{cc} and (b) χ''_{cc} at various frequencies. $h = 50$ mOe. $h \parallel c$.

common to spin glass behaviours. The peak temperature of χ''_{cc} between T_{cu} and T_{cl} slightly shifts to the low temperature side with increasing frequency, while the peak temperature of χ'_{aa} and χ'_{cc} between T_{cu} and T_{cl} remains almost unchanged with frequency.

Figure 6(a) shows the T dependence of χ'_{aa} at various H along the c plane. At fields lower than H'_E (=50 Oe) the peak temperature T_{max} of χ'_{aa} changes with magnetic field in a rather complicated manner. Above H'_E the peak shifts to the high temperature side with

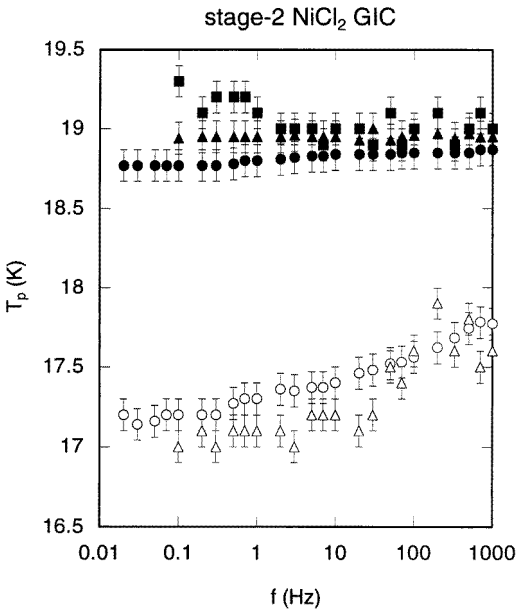

Figure 5. f dependence of peak temperatures T_p in χ'_{aa} (●), χ''_{aa} (○), χ'_{cc} (▲) and χ''_{cc} (△, ■).

further increasing field. This implies that the in-plane ferromagnetic order is apparently enhanced by the application of H. The relations of T_{max} against H and χ'_{max} against H for $70 \leqslant H \leqslant 1000$ Oe can be well described by $T_{max}(H) - T_{max}(0) \approx H^{\mu}$ and $\chi'_{max} \approx H^{-\lambda}$, respectively, with the exponents $\mu = 0.62 \pm 0.02$ and $\lambda = 0.68 \pm 0.03$, where $T_{max}(0)$ is treated as an unknown parameter in the least squares fit.

Figure 6(b) shows that T dependence of χ''_{aa} at various magnetic fields along the c plane. The shoulder around T_{cu} at $H = 0$ disappears even at 1–5 Oe, suggesting that the anisotropy field in the c plane H_A^{in} is of the order of 5 Oe. At fields between H_A^{in} and H'_E the peak of χ''_{aa} at T_{cl} observed at $H = 0$ shifts with magnetic field in a rather complicated manner.

Figures 7(a) and (b) show the H dependence of χ'_{aa} and χ''_{aa} at various T when the magnetic field is applied along the c plane. The absorption χ''_{aa} has three peaks at H_{c0} ($\approx$4 Oe), H_{c1} ($\approx$20 Oe) and H_{c2} ($\approx$35 Oe) at 14 K, while the dispersion χ'_{aa} has only two peaks at H_{c0} and H_{c1}. Figure 7(c) shows the T dependence of H_{c0}, H_{c1} and H_{c2}. The field H_{c0} reduces to zero between 17 and 18 K, while the fields H_{c1} and H_{c2} tend to reduce to zero around 21 K. The magnetic fields H_{c0}, H_{c1} and H_{c2} at 0 K correspond to H_A^{in}, H_{SF} and H'_E, respectively: $H_A^{in} \approx 6$ Oe, $H_{SF} \approx 22$ Oe and $H'_E \approx 40$ Oe. In fact the value of H'_E thus determined is almost the same as that derived from figure 1(c). The value of H_A^{in} is of the same order as that (=10 Oe) reported by Karimov *et al* [1]. The value of H_{SF} coincides with that estimated from the relation $H_{SF} = [2H_A^{in}H'_E]^{1/2}$. Note that the ratio H_{c2}/H_{c1} is 1.82 for stage-2 $NiCl_2$ GIC, which is comparable to that (=2.05) for stage-1 $NiCl_2$ GIC where $H_{c1} = 380$ Oe and $H_{c2} = 780$ Oe [24].

Figures 8(a) and (b) show the f dependence of χ'_{aa} at various temperatures. It is found that χ'_{aa} can be well described by a power-law form ($\chi'_{aa} \approx \omega^{-x}$) over the whole frequency range used in the present work. In figure 8(c) we show a plot of the exponent x as a function of temperature. The exponent x is positive and very close to zero. It may provide

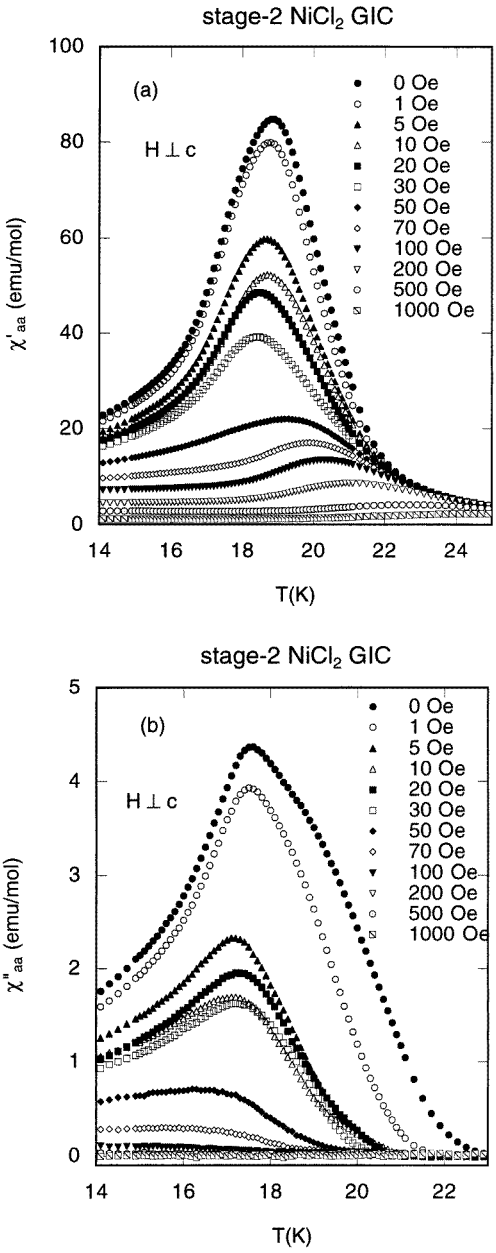

Figure 6. T dependence of (a) χ'_{aa} and (b) χ''_{aa} at various magnetic fields. $H \perp c$. $f = 100$ Hz. $h = 50$ mOe.

an appropriate method to define T_{cu} and T_{cl}: it exhibits local maxima at 16.5 K just below T_{cl} and at 21.1 K just above T_{cu}. Note that such a behaviour of x is also observed near T_{cl} (=6.9–7.1 K) and T_{cu} (=8.9 K) in stage-2 $CoCl_2$ GIC [25].

Figures 9(a), (b), (c), (d) and (e) show the f dependence of χ''_{aa} at various T. The f dependence of χ''_{aa} for $f < 20$ Hz is rather different from that for $f \geqslant 20$ Hz depending

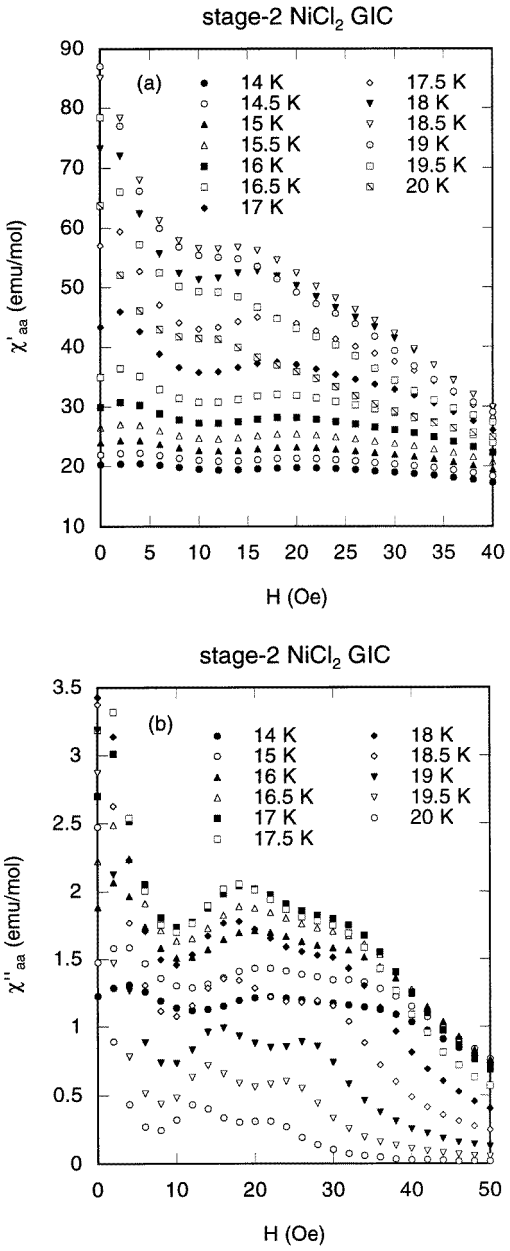

Figure 7. H dependence of (a) χ'_{aa} and (b) χ''_{aa} at various temperatures. (c) T dependence of critical fields H_{c0}, H_{c1} and H_{c2} determined from the data of χ' against H (●, ▲, ■) and χ'_{aa} against H (○, △).

on temperature. The f dependence of χ''_{aa} for $f \leqslant 20$ Hz is summarized as follows. (i) For $T < 16$ K χ''_{aa} decreases with increasing frequency except for small peaks around $f = 0.2$ Hz and 2 Hz. (ii) Around 16.6–16.8 K just below T_{cl} χ''_{aa} is almost independent of frequency. (iii) For $17 \leqslant T \leqslant 19.8$ K χ''_{aa} increases with increasing frequency except for a

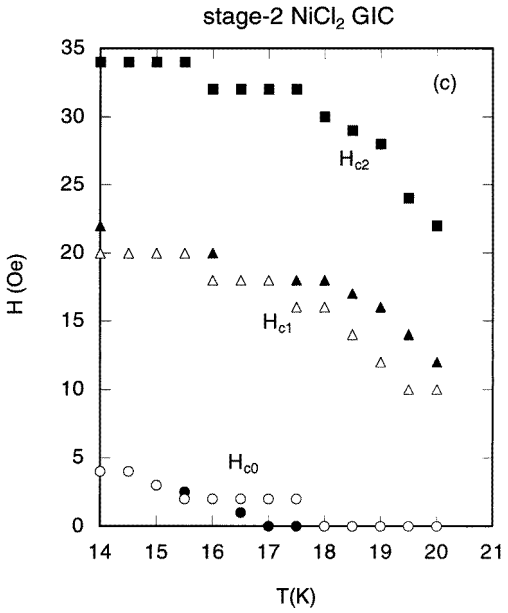

Figure 7. (Continued)

broad peak around 5 Hz. (iv) Around T_{cu} χ''_{aa} becomes constant. (v) For $T > 20.6$ K χ''_{aa} decreases with increasing frequency. In contrast, the f dependence of χ''_{aa} for $f > 20$ Hz is summarized as follows. The absorption χ''_{aa} increases with increasing frequency for $T \leqslant 21$ K and decreases with increasing frequency for $T \geqslant 21.3$ K.

5. Discussion

5.1. Model: relaxation due to intraisland and interisland fluctuations

Here we present a simple model [25] which may explain the f dependence of χ'_{aa} and χ''_{aa} in stage-2 $NiCl_2$ GIC. The magnetization of each island fluctuates with characteristic relaxation times τ_{in} and τ_{out} associated with intraisland and interisland correlations, respectively. Correspondingly the characteristic frequencies f_{in} and f_{out} are defined by $(2\pi\tau_{in})^{-1}$ and $(2\pi\tau_{out})^{-1}$, respectively. When the relaxation of these fluctuations is of Debye type, the dispersion χ'_{aa} and absorption χ''_{aa} may be described by

$$\chi'_{aa}(\omega) = \chi^{in}_{aa}(\boldsymbol{Q}=\boldsymbol{0})\frac{1}{1+(\omega\tau_{in})^2} + \chi^{out}_{aa}(\boldsymbol{Q}=\boldsymbol{0})\frac{1}{1+(\omega\tau_{out})^2} \tag{2}$$

and

$$\chi''_{aa}(\omega) = \chi^{in}_{aa}(\boldsymbol{Q}=\boldsymbol{0})\frac{\omega\tau_{in}}{1+(\omega\tau_{in})^2} + \chi^{out}_{aa}(\boldsymbol{Q}=\boldsymbol{0})\frac{\omega\tau_{out}}{1+(\omega\tau_{out})^2}. \tag{3}$$

Each Ni^{2+} ion is regularly located on the triangular lattice inside the same island. The wavevector dependent susceptibility $\chi^{in}_{aa}(\boldsymbol{Q})$ related to the intraisland fluctuations may be described by

$$\chi^{in}_{aa}(\boldsymbol{Q}) = \langle S^a_{\boldsymbol{Q}}(t=0)S^a_{-\boldsymbol{Q}}(t=0)\rangle_{in} \approx \frac{1}{[(\boldsymbol{Q}-\boldsymbol{G}_a)^2 + (1/\xi^{in}_a)^2]^{(2-\eta)/2}} \tag{4}$$

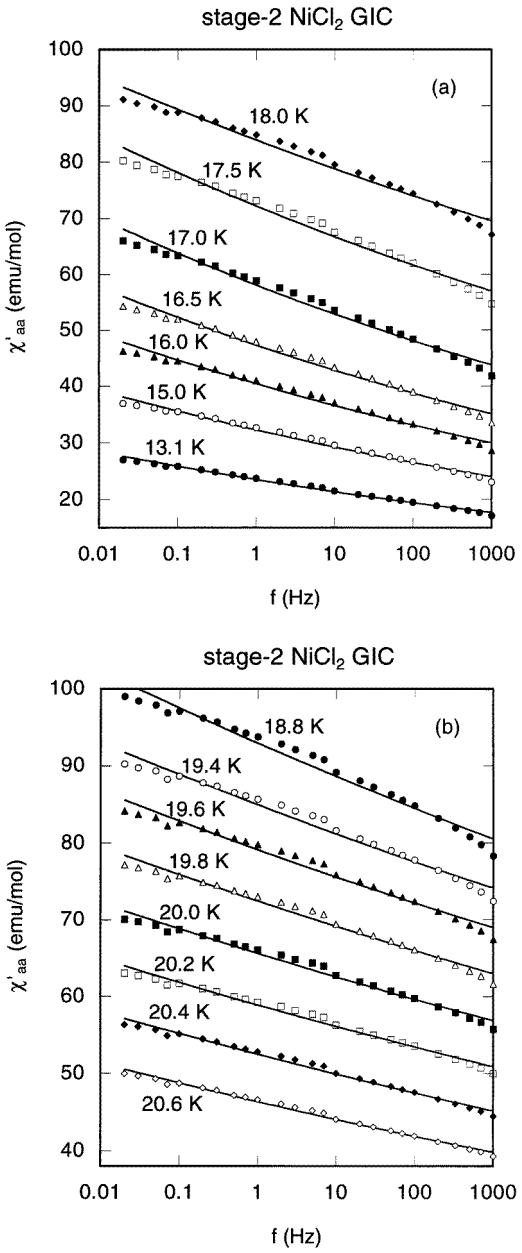

Figure 8. (a) and (b) f dependence of χ'_{aa} at various temperatures. (c) T dependence of exponent x where χ'_{aa} is described by a power law form ($\chi'_{aa} \approx \omega^{-x}$) over the whole frequency range.

where $S^a_{\boldsymbol{Q}}$ is the Fourier transform of spin component S^a_j at the site $\boldsymbol{r}_j$, $\boldsymbol{G}_a$ is the in-plane reciprocal lattice vector, η ($\approx$0) is a critical exponent of Fisher–Burford and ξ^{in}_a is the intraisland spin correlation length. In contrast, there is no coherency of lattice between different islands. The wavevector-dependent susceptibility $\chi^{out}_{aa}(\boldsymbol{Q})$ related to the interisland

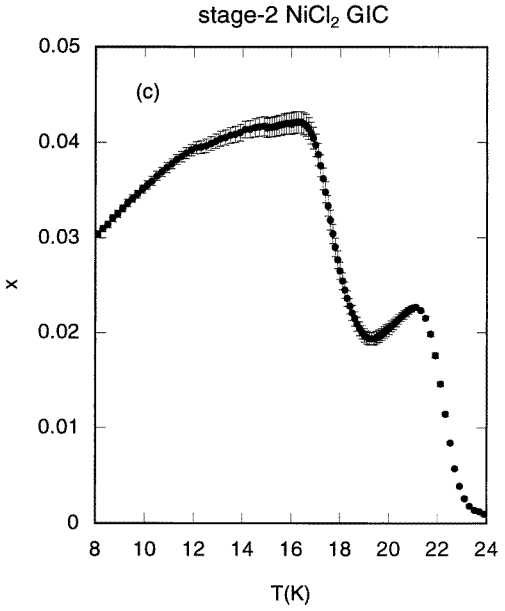

Figure 8. (Continued)

fluctuations may be described by

$$\chi_{aa}^{out}(\boldsymbol{Q}) = \langle S_{\boldsymbol{Q}}^{a}(t=0)S_{-\boldsymbol{Q}}^{a}(t=0)\rangle_{out} \approx \frac{1}{[\boldsymbol{Q}^2 + (1/\xi_a^{out})^2]^{(2-\eta')/2}} \tag{5}$$

where ξ_a^{out} is the interisland spin correlation length and η' ($\approx$0) is a critical exponent of Fisher–Burford. The susceptibility $\chi_{aa}^{in}(\boldsymbol{Q})$ has a peak around each $\boldsymbol{Q} = \boldsymbol{G}_a$, while $\chi_{aa}^{out}(\boldsymbol{Q})$ has a peak only at $\boldsymbol{Q} = \boldsymbol{0}$. The static susceptibilities $\chi_{aa}^{in}(\boldsymbol{Q} = \boldsymbol{0})$ and $\chi_{aa}^{out}(\boldsymbol{Q} = \boldsymbol{0})$ may diverge at T_{cu} and T_{cl}, respectively. In the above derivation the following approximation is used

$$\langle S_{\boldsymbol{Q}=\boldsymbol{0}}^{a}(0)S_{-\boldsymbol{Q}=\boldsymbol{0}}^{a}(t)\rangle = \langle S_{\boldsymbol{Q}=\boldsymbol{0}}^{a}(0)S_{-\boldsymbol{Q}=\boldsymbol{0}}^{a}(0)\rangle \exp\left(-\frac{t}{\tau}\right) \tag{6}$$

where τ is a characteristic relaxation time. The dispersion χ' decreases with increasing ω, being independent of temperature. In contrast the absorption χ'' exhibits maxima at $\omega\tau_{in} = 1$ and $\omega\tau_{out} = 1$ depending on temperature.

5.2. f_{in} and f_{out} estimated from nonlinear susceptibility

What are the orders of f_{in} and f_{out} in stage-2 $NiCl_2$ GIC? The orders of f_{in} and f_{out} have been estimated by Matsuura and Hagiwara [15] and Miyoshi *et al* [17] from their results of nonlinear susceptibility for stage-2 $NiCl_2$ GIC. Their results are summarized as follows. The nonlinear susceptibility χ_2 is defined by $\chi_2 = -4M'_{3\omega}/h^3$ in the limit of $h \to 0$, where $M'_{3\omega}$ is the real part of the third harmonic (3ω) in-phase component of AC magnetization driven by an external AC magnetic field with angular frequency ω ($h\exp(\mathrm{i}\omega t)$). Matsuura and Hagiwara [15] have shown that the nonlinear susceptibility χ_2 at low frequencies of 1 mHz $\leqslant f \leqslant$ 1 Hz has a negative-divergent singularity at T_{cu} (=21 K) and an antisymmetric singularity at T_{cl} (=17 K) where the sign changes from negative

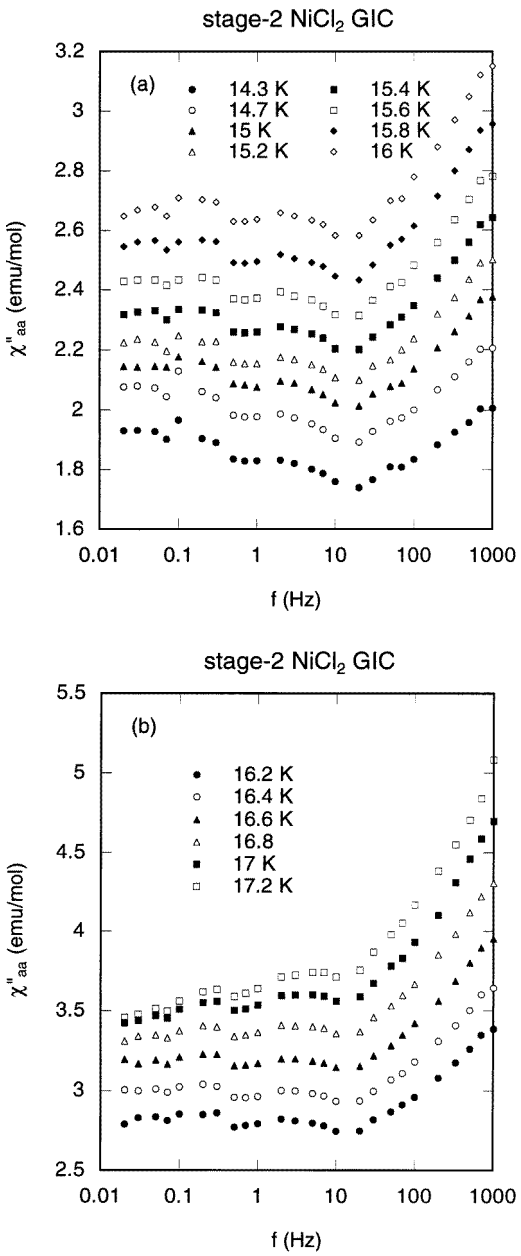

Figure 9. (a)–(e) f dependence of χ''_{aa} at various temperatures.

to positive as the temperature decreases. The change of sign in χ_2 reflects the breaking of spatial magnetic symmetry. The singularity of χ_2 at T_{cl} indicates the appearance of 3D antiferromagnetic phase below T_{cl}. Recently Miyoshi *et al* [17] have measured the T dependence of χ_2 in stage-2 $NiCl_2$ GIC at higher frequencies ($3.7 \leqslant f \leqslant 370$ Hz). They have shown that the singularity of χ_2 at T_{cu} changes from a negative-divergent one for $f < 0.1$ Hz to an antisymmetric one for $37 \leqslant f \leqslant 370$ Hz. The change of sign in χ_2 at

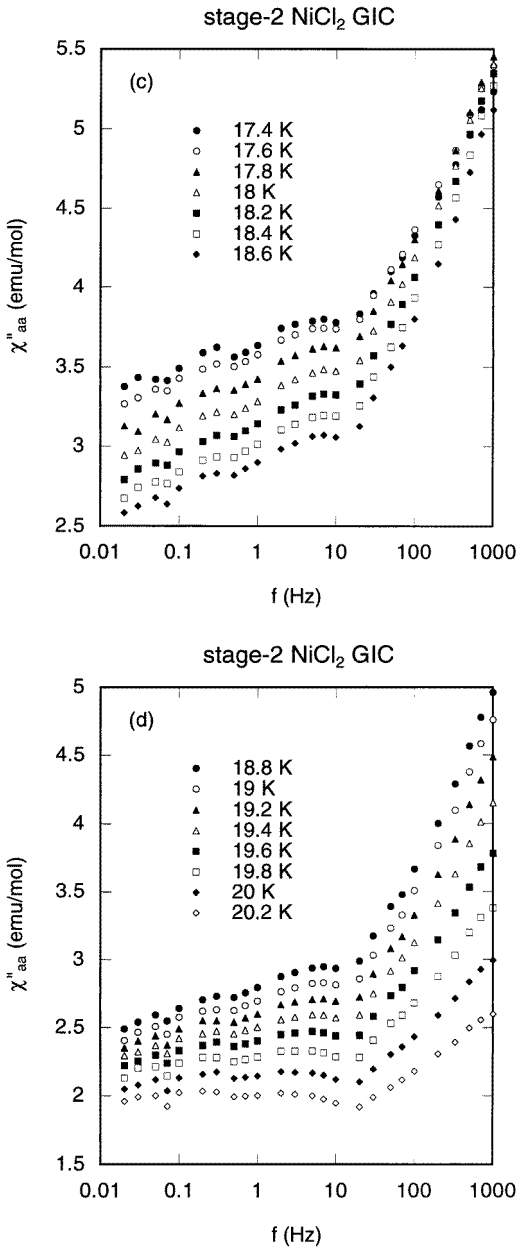

Figure 9. (Continued)

T_{cu} indicates the appearance of 2D ferromagnetic phase below T_{cu}. These results may be explained as follows. The characteristic frequency f_{in} related to the intraisland fluctuations is much higher than the characteristic frequency f_{out} related to the interisland fluctuations. The contribution of intraisland fluctuations to the singularity of χ_2 at T_{cu} can be observed mainly at high frequencies close to $f = f_{in}$, while the contribution of interisland fluctuation to the singularity of χ_2 at T_{cl} can be observed mainly at low frequencies close to $f = f_{out}$.

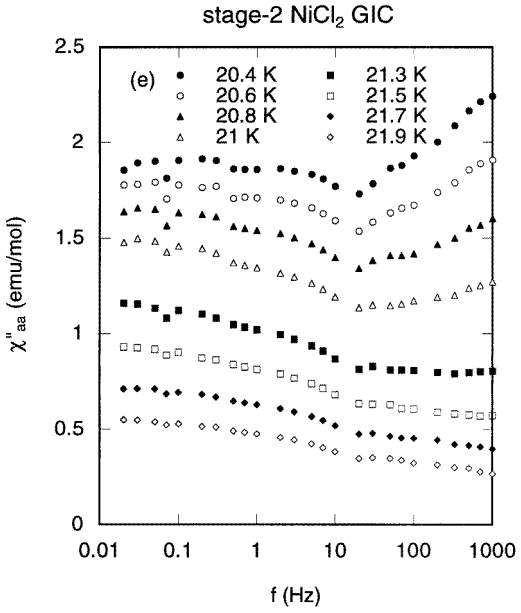

Figure 9. (Continued)

It is concluded from the above result that (i) f_{out} at T_{cl} is of the order of 0.1 Hz and (ii) f_{in} at T_{cu} is at least larger than 37 Hz.

5.3. Frequency dependence of χ'_{aa}

Here we assume that the characteristic frequency f_{in} is much larger than f_{out}. The frequencies f_{in} and f_{out} are expected to increase with increasing temperature. As shown in figure 9 the frequency dependence of χ''_{aa} is separated into two parts: the high frequency part ($f > 20$ Hz) and the low frequency part ($f < 20$ Hz). The high and low frequency parts may mainly correspond to the contributions from intraisland and interisland fluctuations, respectively.

First we discuss the frequency dependence of χ''_{aa} for $0.02 < f < 20$ Hz in terms of the above model. In figure 9(a) χ''_{aa} for $T < 16$ K decreases with increasing frequency. Since $\chi^{out}_{aa}(\boldsymbol{Q} = \boldsymbol{0})$ is larger than $\chi^{in}_{aa}(\boldsymbol{Q} = \boldsymbol{0})$ below T_{cl}, χ''_{aa} is determined mainly by the second term of (3): χ''_{aa} has a peak at $\omega\tau_{out} = 1$. The decrease of χ''_{aa} with increasing frequency suggests that f_{out} is at least lower than 0.02 Hz. In figures 9(b), (c) and (d), χ''_{aa} for $17 < T < 19.8$ K increases with increasing frequency except for a broad peak around 5 Hz. Between T_{cl} and T_{cu} where $\chi^{in}_{aa}(\boldsymbol{Q} = \boldsymbol{0})$ is comparable to $\chi^{out}_{aa}(\boldsymbol{Q} = \boldsymbol{0})$, $\chi''_{aa}(\omega)$ can be approximated by

$$\chi''_{aa}(\omega) = \chi^{in}_{aa}(\boldsymbol{Q} = \boldsymbol{0})(\omega\tau_{in}) + \chi^{out}_{aa}(\boldsymbol{Q} = \boldsymbol{0})\frac{\omega\tau_{out}}{1 + (\omega\tau_{out})^2} \tag{7}$$

since $f \ll f_{in}$. The increase of χ''_{aa} with increasing frequency is due to the first term of (7). The broad peak around 5 Hz is due to the second term of (7), suggesting that f_{out} is nearly equal to 5 Hz. In figure 9(e) χ''_{aa} decreases with increasing frequency for $T > 20.6$ K. Above T_{cu} where $\chi^{in}_{aa}(\boldsymbol{Q} = \boldsymbol{0})$ is larger than $\chi^{out}_{aa}(\boldsymbol{Q} = \boldsymbol{0})$, χ''_{aa} can be still described by (7). If the first term of (7) is smaller than the second term because of $\omega\tau_{in} \ll 1$ and $\omega\tau_{out} \geqslant 1$,

then the decrease of χ''_{aa} with increasing frequency is due to the second term which is proportional to $(\omega\tau_{out})^{-1}$.

Next we discuss the frequency dependence of χ''_{aa} for $20 < f < 1000$ Hz. In figure 9 χ''_{aa} increases with increasing frequency for $T \leqslant 21$ K and decreases with increasing frequency for $T \geqslant 21.3$ K. No peak of χ''_{aa} is observed for $20 < f \leqslant 1000$ Hz, suggesting that f_{in} is much larger than 1 kHz. This result is not inconsistent with the result of Miyoshi *et al* [17] that f_{in} is at least larger than 37 Hz. Since $\omega\tau_{out} \gg 1$ and $\omega\tau_{in} \ll 1$, $\chi''_{aa}(\omega)$ can be approximated by

$$\chi''_{aa}(\omega) = \chi^{in}_{aa}(\boldsymbol{Q} = \boldsymbol{0})(\omega\tau_{in}) + \chi^{out}_{aa}(\boldsymbol{Q} = \boldsymbol{0})(\omega\tau_{out})^{-1}. \tag{8}$$

The increase of χ''_{aa} with increasing frequency for $T \leqslant 21$ K is due to the first term of (8), while the decreases of χ''_{aa} with increasing frequency is due to the second term of (8).

In summary there are two kinds of characteristic frequencies associated with intraisland fluctuation (f_{in}) and interisland fluctuations (f_{out}). The characteristic frequency f_{in} is higher than 1 kHz at least for $T < 22$ K. The characteristic frequency f_{out} is around 5 Hz between T_{cl} and T_{cu}, decreases with decreasing temperature and becomes less than 0.02 Hz below T_{cl}. Since $\tau_{out} = (2\pi f_{out})^{-1}$, the decrease of f_{out} implies the increase of relaxation time τ_{out} near T_{cl}, which is a feature common to spin glasses near the freezing temperature [26].

5.4. Frequency dependence of χ'_{aa}

We discuss the frequency dependence of χ'_{aa} in terms of the above model. Since the condition $\omega\tau_{in} \ll 1$ is satisfied for $0.02 \leqslant f \leqslant 1000$ Hz, the frequency dependence of χ'_{aa} is determined mainly by the second term of (2). The absorption χ'_{aa} below T_{cl} is proportional to $(\omega\tau_{out})^{-2}$ since $\omega\tau_{out} \gg 1$ and becomes weakly dependent on frequency with increasing temperature because of the decrease in τ_{out} with temperature. In contrast, as shown in figure 8(c), the measured exponent x ($\chi'_{aa} \approx \omega^{-x}$) is much smaller than that predicted from (2), suggesting that (2) is not a correct expression of χ'_{aa} in stage-2 $NiCl_2$ GIC at least concerning the frequency dependence. When the power law form ($\chi'_{aa} \approx \omega^{-x}$) is valid for any frequency, the absorption χ''_{aa} can be calculated as

$$\chi''_{aa}(\omega) \approx \frac{\pi x}{2}\chi'_{aa}(\omega)\mathrm{sgn}(\omega) \tag{9}$$

using the Kramers–Kronig relation

$$\chi''_{aa}(\omega) = -\frac{1}{\pi}P\int_{-\infty}^{\infty} \mathrm{d}\omega' \, \frac{1}{\omega' - \omega}[\chi'_{aa}(\omega') - \chi^{\infty}_{aa}] \tag{10}$$

where the notation sgn which is 1 for $\omega > 0$ and -1 for $\omega < 0$ is included in (9) because χ''_{aa} should be an odd function of ω, and χ^{∞}_{aa} is the complex susceptibility at $\omega = \infty$ and is assumed to be zero here. As shown in figure 8(c) the temperature dependence of x is similar to that of χ''_{aa}. The ratio χ''_{aa}/χ'_{aa} is roughly equal to 2.4/100 (=0.024) at 18.9 K for $f = 0.02$ Hz, which is of the same order as $\pi x/2$ (=0.03 for $x = 0.02$). Thus these results are consistent with the predictions from (9). The similarity between χ''_{aa} and x suggests a possibility that the critical temperatures T_{cu} and T_{cl} can be determined from the T dependence of x. In fact the exponent x has two peaks at 16.5 K and 21.1 K, while χ''_{aa} has a peak at T_{cl} (=17.2 K) and a shoulder at T_{cu} (=20.5 ± 0.2 K). Note that x has a local minimum at 19.3 K, corresponding to the peak temperature of χ''_{cc} at $f = 0.1$ Hz.

According to the fluctuation–dissipation theorem, the Fourier spectrum $S_{aa}(\omega)$ of the time-dependent magnetization fluctuation $\langle M_a(0)M_a(t)\rangle$ is related to $\chi''_{aa}(\omega)$ by

$$S_{aa}(\omega) = \int_{-\infty}^{\infty} \langle M_a(0)M_a(t)\rangle \, \mathrm{e}^{-\mathrm{i}\omega t} \, \mathrm{d}t = \frac{2k_B T}{\hbar\omega}\chi''_{aa}(\omega) \tag{11}$$

where $M_a(t)$ is the time-dependent magnetization along the c plane. It is expected from (9) that, below T_{cl}, χ''_{aa} at low frequencies is described by the same power law form as χ'_{aa} ($\chi''_{aa} \approx \omega^{-x}$). Thus $S_{aa}(\omega)$ has the form $\omega^{-(1+x)}$, indicating that $\langle M_a(0)M_a(t)\rangle$ varies with t as t^x. In the limit of $x \to 0$, $\langle M_a(0)M_a(t)\rangle$ has a logarithmic time dependence. As shown in figure 2, at temperatures sufficiently lower than T_{cl} the magnetization M_a^{ZFC} along the c plane is much smaller than the magnetization M_a^{FC} which is one at thermal equilibrium. The magnetization M_a^{ZFC} may increase and reach M_a^{FC} with t as $\ln(t)$.

In summary the time-dependent magnetization fluctuation $\langle M_a(0)M_a(t)\rangle$ varies with t as t^x. The exponent x as a function of temperature clearly shows a very broad peak at T_{cu} and a sharp peak at T_{cl}, which may provide a better method for determining the critical temperatures compared to that of χ''_{aa}: χ''_{aa} has a broad peak at T_{cl} and a shoulder at T_{cu}. The exponent x is very close to zero. The value of $x = 0$ has been reported in many spin glasses [26].

5.5. Origin of cluster-glass-like phase

We have seen that the 3D antiferromagnetic phase appears below T_{cl}. As shown in figure 5, the critical temperature T_{cl} identified with the peak temperature of χ''_{aa} and χ''_{cc} shifts to the high temperature side with increasing frequency. This feature, which is common to spin glass behaviours, suggests that the ordered phase below T_{cl} may have the characteristic of a cluster-glass-like phase. The magnetization of each ferromagnetic island near T_{cl} fluctuates with the relaxation time τ_{out}, which increases with decreasing temperature. Each island plays a role of spins in the spin glass behaviour. The spin directions of ferromagnetic islands may be partly frozen because of frustrated interisland interactions. In figure 2 we show that an irreversible effect of magnetization occurs below T_f which is higher than T_{cl}. This may be further evidence for such a cluster-glass phase.

What is the origin of such frustrated interisland fluctuations causing the cluster-glass-like phase? It may arise from the competition among the frustrated interisland interactions: (i) the dipole–dipole interaction between adjacent islands in the same intercalate layer and (ii) the effective antiferromagnetic interplanar exchange interaction between islands in different intercalate layers. The dipole–dipole interaction is approximately given by [27]

$$E_d^{AF} = \frac{\pi^2 g^2 \mu_B^2 S^2 L}{12a^4} \tag{12}$$

for the antiferromagnetic alignment, where L is a diameter of ferromagnetic islands and also the distance between centres of adjacent islands. The effective interplanar exchange interaction may be described by [27]

$$J'_{eff} \approx J' S(S+1) p \frac{\pi L^2}{2\sqrt{3}a^2} \tag{13}$$

where a is the in-plane lattice constant and p ($0 < p < 1$) is the degree of the overlapping of one ferromagnetic island of diameter L in an intercalate layer with another island of the same diameter in the nearest neighbour adjacent intercalate layers. Here we define the diameter L_c by

$$L_c = \frac{\sqrt{3}}{6pa^2} \frac{g_a^2 \mu_B^2 S}{|J|(S+1)} \left| \frac{J}{J'} \right| \tag{14}$$

where the effective interplanar exchange interaction ($|J'_{eff}|$) is of the same order as that of the dipole–dipole interaction ($|E_d^{AF}|$). When L is much larger than L_c, the effective interplanar interaction dominantly contributes to the frustrated interisland interaction. When L is

much smaller than L_c, the dipole–dipole interaction dominantly contributes to the frustrated interisland interaction. The value of L_c is estimated as $L_c \approx 0.096|J/J'|$ (Å) = 116 Å for the stage-2 $NiCl_2$ GIC where $J = 7.26$ K, $J' = -6 \times 10^{-4}$ K, $S = 1$, $g_a = 2.156$, $a = 3.46$ Å and $p = 1/2$. This value of L_c is of the same order as the diameter of small islands (≈130–170 Å) which is determined from neutron small angle scattering by Flandrois *et al* [28]. This implies that both the dipole–dipole interaction and the effective interplanar interaction contribute to the frustrated interisland interaction. The effective antiferromagnetic interplanar interaction becomes dominant below T_{cl}, leading to the 3D antiferromagnetic order.

6. Conclusion

Stage-2 $NiCl_2$ GIC magnetically behaves like a quasi-2D XY-like ferromagnet with very weak antiferromagnetic exchange interaction. The spin Hamiltonian is given by (1) with $J = 7.26 \pm 0.05$ K, $D = 0.28$ K and $J' = -6 \times 10^{-4}$ K. The magnetic phase transitions of stage-2 $NiCl_2$ GIC have been studied by AC SQUID magnetic susceptibility. This compound undergoes magnetic phase transitions at T_{cl} (=17.2 K) and T_{cu} (=20.5 ± 0.2 K). Between T_{cu} and T_{cl} a 2D long range order is established within each island in the intercalate layer. The ordered phase below T_{cl} is a 3D antiferromagnetic one with the frustrated nature of cluster-glass-like behaviour. The spin directions of ferromagnetic islands may be partly frozen because of frustrated interisland interactions.

Acknowledgments

We would like to thank H Suematsu for providing us with single crystal kish graphite. We are also grateful to J K Woo for sample characterization and to C R Burr for a critical reading of this manuscript. This work was partly supported by NSF DMR 9625829.

References

[1] Karimov Yu S, Vol'pin M E and Novikov Yu N 1971 *JETP Lett.* **14** 142–4
[2] Karimov Yu S and Novikov Yu N 1974 *JETP Lett.* **19** 159–60
[3] Karimov Yu S 1974 *Sov. Phys.–JETP* **38** 129–33
[4] Karimov Yu S 1974 *Sov. Phys.–JETP* **39** 547–50
[5] Karimov Yu S 1975 *Sov. Phys.–JETP* **41** 772–6
[6] Flandrois S, Amiell J and Masson J-M 1980 *Phys. Lett.* **80A** 328–30
[7] Suzuki M and Ikeda H 1981 *J. Phys. C: Solid State Phys.* **14** L923–8
[8] Onn D G, Alexander M G and Flandrois S 1982 *J. Appl. Phys.* **53** 2751–3
[9] Suzuki M, Ikeda H, Murakami Y, Matsuura M, Suematsu H, Nishitani R and Yoshizaki R 1983 *J. Magn. Magn. Mater.* **31–34** 1173–4
[10] Suzuki M, Murata M and Suematsu H 1983 *Synth. Met.* **6** 173–84
[11] Suematsu H, Nishitani R, Yoshizaki R, Suzuki M and Ikeda H 1983 *J. Phys. Soc. Japan* **52** 3874–85
[12] Flandrois S, Masson J-M, Rouillon J-C, Gaultier J and Hauw C 1983 *Synth. Met.* **3** 1–13
[13] Suzuki M, Koga K and Jinzaki Y 1984 *J. Phys. Soc. Japan* **53** 2745–51
[14] Wiesler D G, Suzuki M and Zabel H 1987 *Phys. Rev.* B **36** 7051–62
[15] Matsuura M and Hagiwara M 1990 *J. Phys. Soc. Japan* **59** 3819–22
[16] Chehab S, Biensan P, Flandrois S and Amiell J 1992 *Phys. Rev.* B **45** 2844–54
[17] Miyoshi K, Hagiwara M and Matsuura M 1996 *J. Phys. Soc. Japan* **65** 3306–11
[18] Lines M E 1963 *Phys. Rev.* **131** 546–55
[19] Starr C, Bitter F and Kaufmann A R 1940 *Phys. Rev.* **58** 977–83
[20] Katsumata K and Yamasaka K 1973 *J. Phys. Soc. Japan* **34** 346–52
[21] Billerey D, Terrier C, Pointon A J and Redoules J P 1980 *J. Magn. Magn. Mater.* **21** 187–90

[22] Lindgård P A, Birgeneau R J, Als-Nielsen J and Guggenheim H J 1975 *J. Phys. C: Solid State Phys.* **8** 1059–69
[23] Flandrois S, Amiell J, Agricole B, Stumpp E, Ehrhardt C and Schubert P 1989 *Synth. Met.* **34** 531–6
[24] Nicholls J T, Speck J S and Dresselhaus G 1989 *Phys. Rev.* B **39** 10 047–55
[25] Suzuki M and Suzuki I S 1998 *Phys. Rev.* B **58** at press
[26] Mydosh J A 1993 *Spin Glasses: an Experimantal Introduction* (London: Taylor and Francis)
[27] Suzuki I S, Suzuki M and Maruyama Y 1993 *Phys. Rev.* B **48** 13 550–8
[28] Flandrois S, Hewat A W, Hauw C and Bragg R H 1983 *Synth. Met.* **7** 305–12